Bubble Acceleration in the Ablative Rayleigh-Taylor Instability

R. Betti and J. Sanz*

*Fusion Science Center for Extreme States of Matter and Fast Ignition Physics, Laboratory for Laser Energetics,
University of Rochester, 250 East River Road, Rochester, New York 14623, USA*

The highly nonlinear evolution of the single-mode Rayleigh-Taylor instability (RTI) at the ablation front of an accelerated target is investigated in the parameter range typical of inertial confinement fusion implosions. A new phase of the nonlinear bubble evolution is discovered. After the linear growth phase and a short constant-velocity phase, it is found that the bubble is accelerated to velocities well above the classical value. This acceleration is driven by the vorticity accumulation inside the bubble resulting from the mass ablation and vorticity convection off the ablation front. While the ablative growth rates are slower than their classical values in the linear regime, the ablative RTI grows faster than the classical RTI in the nonlinear regime for deuterium and tritium ablators.

In inertial confinement fusion (ICF), a dense shell of cryogenic deuterium and tritium (DT) is accelerated inward by direct laser irradiation or by the x ray emitted by a high-Z enclosure [1]. The radiation absorbed by the target material causes mass ablation off the shell outer surface, resulting in an inward momentum input leading to the shell acceleration. It is during this acceleration phase that the outer shell surface is unstable to the Rayleigh-Taylor instability (RTI), which occurs when a less dense ("lighter") fluid (ablated plasma) is pushing on a denser ("heavier") fluid (the unablated plasma) and develops as an interchange instability, where "bubbles" of lighter fluid "rise" through the denser fluid, which falls through the lighter fluid in the form of narrow "spikes." Because of RTI, nonuniformities in the target illumination and shell surfaces would grow exponentially in time during the linear phase. The integrity of the dense shell is compromised as the RTI bubbles approach the inner shell surface. The estimate for when this will happen naturally depends on the bubble velocity through the dense fluid. The work presented here yields the single-mode bubble velocity including finite vorticity effects. Such effects are important when the bubble vertex has traveled a distance comparable to the bubble width.

The classical theory [2] (i.e., without ablation) of a heavy fluid of density ρ_h supported by a lighter fluid of density ρ_l in a gravitational field g yields linear growth rates $\gamma_{cl} = \sqrt{A_T k g}$, where $k = 2\pi/\lambda$ is the perturbation wave number, and $A_T = (\rho_h - \rho_l)/(\rho_h + \rho_l)$ is the Atwood number. Because of mass ablation, the classic RTI growth rate is significantly reduced [3,4]. When ablation is included, the growth rate can be approximated [3] by $\gamma_{abl} \approx \sqrt{kg - \rho_h k^2 V_a^2/\rho_l} - 2kV_a$, where $V_a = \dot{m}_a/\rho_h$ is the ablation velocity defined as the ratio between the ablation rate $\dot{m}_a$ and the peak shell density ρ_h, and ρ_l is the so-called blowoff density given by [3] $\rho_l \approx \rho_h(kL_m\beta)^{1/\nu} \ll \rho_h$. Here L_m is the minimum density gradient scale length, ν is the power index for thermal

conduction, and $\beta \equiv 2\nu^{\nu-1}/(\nu + 1)^{\nu+1}$. The main stabilizing mechanism induced by ablation is the spike fall deceleration caused by the large momentum flux, building up at the spikes due to the local increase of the heat flux. For a DT ablator (direct drive), the linear growth rates can be fit by a simple formula [4] $\gamma \approx 0.94\sqrt{kg} - 2.7kV_a$. Using values of $g \approx 110\ \mu\text{m/ns}^2$ and $V_a = 3.5\ \mu\text{m/ns}$ typical of direct-drive ignition targets leads to an unstable spectrum with a cutoff wavelength of about 5 μm. The effect of ablative reduction in growth rate can be obtained only with significant convection from the ablation front of considerable vorticity. While in classical RTI, the vorticity is generated at the interface and remains localized there, in ablative RTI, the ablative flow removes this vorticity and carries it into the light fluid region, where it affects the bubble dynamics.

It is shown here that the vorticity convection, which is stabilizing in both the linear and the early nonlinear regimes, causes a destabilization of the bubble in the deeply nonlinear phase. Previous nonlinear theories [5] correctly predict the bubble behavior in the early nonlinear stage but fail in this highly nonlinear phase when the vorticity dominates the flow field inside the bubble. The vorticity accretion inside the bubble develops when the peak-to-valley amplitude is of the order of the wavelength. At this point, the mass ablation is predominant at the spikes with respect to the bubble vertex where the plasma is relatively cold. At the spikes, the lateral ablation induces a transversal component to the velocity, thus generating vorticity. The bubble is soon filled with mass at a density approximately equal to the blowoff (or light fluid) density predicted by the linear theory and equal to ρ_l. As the bubble is filled with this lower-density plasma, the heat front cannot penetrate to the bubble vertex and a new ablation front is established between the spikes. Both temperature and density develop a plateau inside the bubble, and the heat flux is mainly absorbed at the new ablation front extending between the spikes. Since ablation becomes negligible at the bubble vertex, the bubble becomes classical and advances inside

the unperturbed target with the classical 2D bubble veloc-
ity [5,6] $U_b^{cl2D} = \sqrt{g(1 - r_d)/3k}$, where $r_d = \rho_l/\rho_h$ is the
density ratio between the bubble density ρ_l and the sur-
rounding heavy fluid density ρ_h. Notice that this is the
bubble penetration velocity with respect to the cold target
material as derived from the classical theory for potential
flow [6]. In this classical phase, the bubble is driven by the
standard balance between buoyancy and drag force.
However, as the bubble rises at constant velocity, more
lower-density plasma is sucked in. Such a lower-density
plasma is produced by mass ablation and carries a large
vorticity $\omega \approx kV_a/r_d$. As the ablated material fills the
bubble, the vorticity increases and the bubble velocity no
longer follows the predictions of the potential theory. In a
two-dimensional bubble, the vorticity must vanish at the
bubble axis, and the bubble volume is filled by two regions
of opposite vorticity on the two sides of the bubble axis
(Fig. 1 shows only the left half of the 2D Cartesian bubble).
In a three-dimensional bubble, the vorticity accumulates
inside a torus aligned along the bubble axis. If vorticity is
present inside the bubble, the buoyancy increases due to
the centrifugal forces which are directed against the accel-
eration g near the bubble vertex. In 2D geometry, this effect
can be easily described by approximating the flow inside
the bubble using two counterrotating vortices with radius
$R \approx \lambda/2 \approx 3/k$ (Fig. 1). Let us assume a rigid rotation
near the bubble boundary with an angular frequency Ω
(vorticity $\omega_0 = 2\Omega$) and velocity $v \sim \Omega R$. In the vicinity
of the bubble vertex, the centrifugal force $\mathbf{F}_c$ is directed
along the positive y direction and opposite to the inertial
force g. The total force per unit volume acting on the
bubble fluid element is $\rho_l(g - \omega_0^2 R/4)$, and the bubble
buoyancy force is increased from $\rho_h g - \rho_l g$ to $\rho_h g -
\rho_l(g - \omega_0^2 R/4) = \rho_h[(1 - r_d)g + r_d\omega_0^2 R/4]$. It follows
that the bubble velocity U_b^{cl2D} given above needs to be
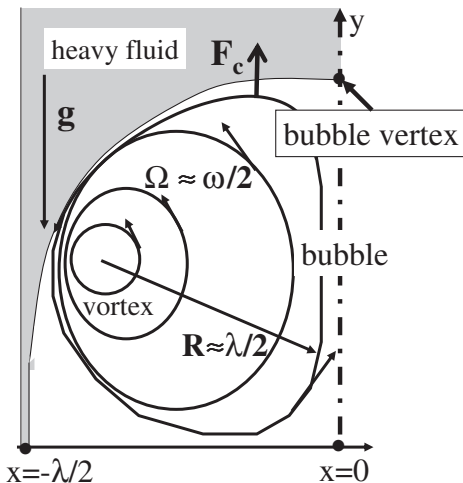modified by adding the rotational term yielding

FIG. 1. Sketch of a vortex located inside half of the bubble.
The vortex has a radius of about $\lambda/2$ and rigid rotation frequency
Ω equal to half the vorticity.

$$U_b^{rot2D} \approx \sqrt{\frac{g(1 - r_d)}{3k} + r_d\frac{\omega_0^2}{4k^2}}. \quad (1)$$

Notice that the rotational term is positive and leads to a
bubble velocity that is larger than the classical value.
Although r_d is usually small, the correction to the classical
value is large since the vorticity convected inside the
bubble scales as $\omega_0 \sim kV_a/r_d$. For wave numbers $k \sim
gr_d/V_a^2$, the vorticity correction is comparable to the clas-
sical term. In this Letter, we show that Eq. (1) is verified by
an analytic theory and 2D simulations.

We start our analysis from a simple analytic model of the
bubble dynamics similar to the one in Ref. [6]. We consider
two incompressible fluids ($j = h, l$) of densities ρ_j. Its
velocity field $\vec{v}_j$ satisfies $\vec{\nabla} \cdot \vec{v}_j = 0$. In a frame of refer-
ence moving with the unperturbed target, the momentum
equation reads $\rho_j(\partial_t\vec{v}_j + \vec{v}_j \cdot \nabla\vec{v}_j) = -\vec{\nabla}p_j - \rho_j g\vec{e}_y$,
where p_j is the pressure, $g\vec{e}_y$ is the target acceleration,
and $\vec{e}_y$ is the unit vector along the y direction. The interface
separating both fluids $y = \eta(x, t)$ is expanded very close to
the vertex of the bubble $x = 0$ as $\eta(x, t) = a(t) - \alpha(t)x^2$,
where the functions of time $a(t)$ and $[2\alpha(t)]^{-1}$ represent
the bubble amplitude and the bubble curvature, respec-
tively. In the surrounding heavy fluid ($j = h$) the flow is
potential, $\vec{v}_h = \vec{\nabla}\Phi$ and $\nabla^2\Phi = 0$. Under a Layzer-type
approximation, the potential Φ can be written as $\Phi =
\Phi_1(t)e^{-ky}\cos(kx)$. For the low-density fluid inside the
bubble, we consider a rotational flow with vorticity $\omega\vec{e}_z \equiv
\vec{\nabla} \times \vec{v}_l$. The stream function Ψ ($\vec{v}_l = \vec{\nabla}\Psi \times \vec{e}_z$) satisfies
$\nabla^2\Psi = -\omega$. Next, we take the simple ansatz for the
vorticity as $\omega = -\omega_0(t)\sin(kx)$. The solution for the
stream function under a Layzer-type approximation is $\Psi =
-\mu(t)x + [\Psi_1(t)e^{ky} - k^{-2}\omega_0(t)]\sin(kx)$. The equation of
the interface is determined from the requirement that sur-
face particles move with the fluid; then, at $y = \eta(x, t)$, the
kinematic conditions $\partial_t\eta + (\vec{v}_j \cdot \vec{e}_x)\partial_x\eta = \vec{v}_j \cdot \vec{e}_j$ must be
verified. Expanding these equations until $O(x^2)$, we find:
$\alpha(t) = k(1 - C_0e^{-3ka})/6$, $\Phi_1(t) = -\dot{a}e^{ka}/k$, $\mu(t) = \dot{a} -
\omega_0/k + (\omega_0 - 2\dot{\alpha}k^{-1})/(k + 6\alpha)$, and $\Psi_1(t) =
k^{-1}e^{-ka}(\omega_0 - 2\dot{\alpha}k^{-1})/(k + 6\alpha)$. Here the dot denotes
the time derivative and C_0 is a constant. Finally, the pres-
sure must be continuous across the interface, $p_h = p_l$ at
$y = \eta(x, t)$. Integrating the momentum equation and ex-
panding until $O(x^2)$, the $O(x^2)$ term yields the relevant
equation. In the deeply nonlinear phase, when the bubble
amplitude is a significant fraction of the mode wavelength,
we find $\alpha \approx k/6$, and $p_h = p_l$ yields

$$\ddot{a} = \frac{[4(1 - r_d)g + 3r_d\omega_0^2/k - 12\dot{a}^2k + 6r_d\dot{\omega}_0^2/k]}{(8 + 4r_d)}. \quad (2)$$

Notice that the steady state asymptotic bubble velocity
obtained from Eq. (2), when $\dot{\omega}_0 \approx 0$ and $\ddot{a} \approx 0$, reprodu-
ces the result given in Eq. (1), $\dot{a}(t \to \infty) \approx U_b^{rot2D}$.

The same procedure can be applied to the bubble evo-
lution in 3D geometry by assuming cylindrical symmetry

of the bubble around the y axis and a flow without azimuthal motion. We take r and θ as the radius and azimuthal angle, respectively, in cylindrical coordinates. The velocity potential for the heavy fluid takes the form $\Phi = \Phi_1(t)J_0(kr)e^{-ky}$, where J_0 is the Bessel function of zeroth order. For the rotational light fluid, the vorticity is $\vec{\omega} = \omega e_\phi = \vec{\nabla} \times \vec{v}_l$, where $\vec{e}_\phi$ is the azimuthal unit vector. The stream function $\Psi(r, y, t)$ $[\vec{v}_l = r^{-1}\vec{\nabla}\Psi \times \vec{e}_\phi]$ satisfies $\nabla^2\Psi - 2r^{-1}\partial_r\Psi = -r\omega$. We consider a simple ansatz for the vorticity as $\omega = \omega_0(t)J_1(kr)$, where J_1 is the Bessel function of first order. Under a Layzer-type approximation, Ψ can be written as $\Psi = \mu(t)r^2/2 + [\Psi_1(t)e^{ky} + k^2\omega_0(t)]rJ_1(kr)$. A similar expansion to the 2D geometry case, up to second order in $r[\eta = a(t) - \alpha(t)r^2]$, yields the asymptotic bubble velocity $U_b^{\text{rot3D}} = \dot{a}(t \rightarrow \infty)$

$$U_b^{\text{rot3D}} \approx \sqrt{\frac{g(1 - r_d)}{k} + r_d\frac{\omega_0^2}{4k^2}}. \quad (3)$$

This model can also be applied to determine the bubble velocity in the ablative Richtmyer-Meshkov (RM) [7] and Darrieus-Landau [8] instabilities where the vorticity-induced acceleration leads to an asymptotic bubble velocity $U_b \sim V_a\sqrt{\rho_h/\rho_c}$. Likely, such a large asymptotic velocity is never achieved in the RM phase of ICF implosions, since the distance between the critical and ablation surface d_c grows quickly, leading to $kd_c > 1$ and decoupling of the critical from the ablation surface over a time scale shorter than the linear growth time. In ICF, the bubble acceleration is therefore relevant to the RTI only.

In order to capture the detailed evolution of the single-mode RTI, we have developed a specialized code (ART) suitable for high resolution simulations of the nonlinear ablative RTI in direct-drive targets. ART solves the single-fluid equations of motion including Spitzer thermal conduction and the ideal gas equation of state over a Cartesian grid. In the absence of a 2D perturbation, the ablation front is kept in quasiequilibrium by a gravitational field with acceleration $\vec{g}$ balancing the ablation pressure. The ablation velocity is initially assigned and the heat flux corresponding to such a mass ablation rate is computed by solving the equilibrium equations. Since the foil mass decreases due to ablation, the acceleration $g(t)$ is slowly varied in time to keep the ablation front approximately fixed in space. This is equivalent to solving the fluid equations in the frame of reference of the accelerated foil. The heat flux is assigned at the boundary of the computational box $y = 0$ in order to maintain constant ablation rate and ablation pressure. In order to explore the nonlinear RTI evolution for configurations of relevance to direct-drive ICF, we have chosen initial hydroprofiles (Fig. 2) of a DT ablator similar to those of a 1.5 MJ direct-drive ignition target [9] during the acceleration phase. In such a target, the DT density of the overdense target follows a monotonically decreasing profile of the kind $\rho = \rho_h(1 - \bar{y}/d)^{3/2}$, where $d = 5P_a/(2\rho_h g)$ is the target thick-
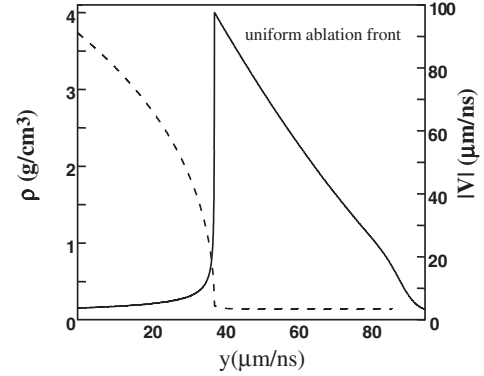

FIG. 2. Density (solid line) and velocity (dashed line) profiles of a 1.5 MJ ignition target [9] during the acceleration phase.

ness, $\rho_h \approx 4$ g/cm³ is the peak density at the ablation front, $P_a \approx 130$ Mb is the pressure at the ablation front, $g(0) \approx 110$ μm/ns², $\bar{y} = y - y_a$, and $V_a \approx 3.5$ μm/ns. Figure 2 shows the equilibrium profiles for the ignition target used in the code ART. A divergence-free velocity perturbation of 1 μm/ns is introduced near the ablation front $y_a \approx 38$ μm at time $t = 0$. The ART simulation is carried out within a computational box of 95 μm in y and 5 μm in x. The width in x is chosen to simulate half of 10 and 7 μm wavelength perturbations. The initial ablation front thickness is about 0.18 μm. In order to resolve such a sharp ablation front, the required computational mesh has 4000 grid cells in y and 210 in x. The bubble penetration velocity U_b is computed as the velocity of the vertex of the bubble relative to the velocity of the dense target plasma averaged in x. The computed bubble velocity is compared with the classical value $U_b^{\text{cl2D}} = \sqrt{g(1 - r_d)/3k}$, where $r_d = \rho_l/\rho_h$. The density ρ_h is the maximum density at the bubble vertex, while ρ_l is the density at a distance $2/k$ below the vertex as indicated by the linear theory [3]. To compare the results of the simulation with the theory, we
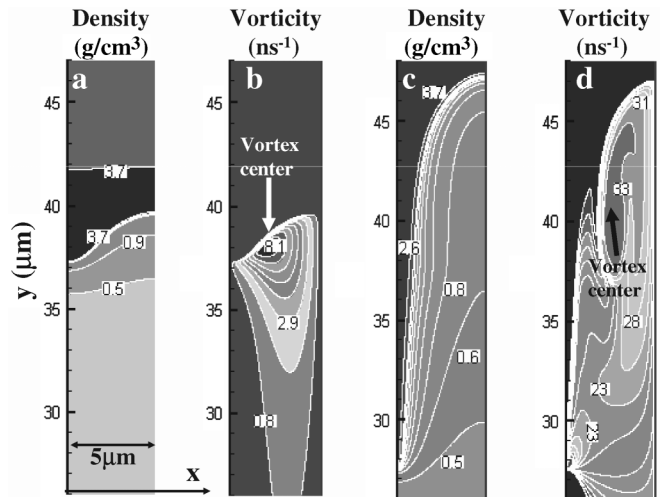

FIG. 3. Contour plots of the (a),(c) density and (b),(d) vorticity at (a),(b) 1 and (c),(d) 2.25 ns into the acceleration phase for $\lambda = 10$ μm. The density $1/e$ point is at 62 μm.
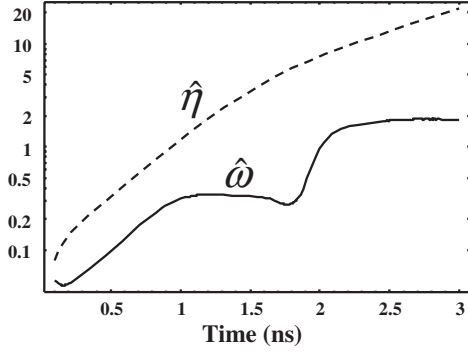
FIG. 4. Half the peak-to-valley amplitude $\hat{\eta}$ normalized with 0.1λ (dashed line) for $\lambda = 10\ \mu$m. Vorticity at the bubble vertex normalized with kV_a/r_d (solid line).

compute the vorticity to use into Eq. (1). The vorticity near the bubble vertex is taken as the volume average of $\vec{\nabla} \times \vec{v}$ inside half the bubble between the bubble vertex and the distance $1/k$ from the vertex into the bubble. Figure 3 shows the contour plots of the density and the vorticity inside the bubble at 1 and 2.25 ns for $\lambda = 10\ \mu$m. At 1 ns [Figs. 3(a) and 3(b)], the RTI approaches the classical saturation where the amplitude is about 0.1λ. At this time, the RTI vortex is centered about the midpoint between the spike tip and the bubble vertex [Fig. 3(b)]. At 2.25 ns [Fig. 3(c) and 3(d)], the mode amplitude is about equal to the wavelength. At this highly nonlinear stage, the RTI vortex has climbed towards the bubble vertex. Most of the vorticity is now produced near the tip of the spike and is convected towards the bubble vertex by the plasma flowing into the bubble [Fig. 3(d)]. Near the bubble vertex, the magnitude of the vorticity reaches 27 ns^{-1}. The evolution of the normalized vorticity near the bubble vertex $\hat{\omega} = \omega/(kV_a/r_d)$ is shown in Fig. 4 together with half the peak-to-valley amplitude η normalized with the classical saturation amplitude $\hat{\eta} = \eta/0.1\lambda$. After a period of saturated vorticity at around 1 ns, the vorticity increases rapidly as the RTI vortex reaches the bubble vertex. Figure 5 shows
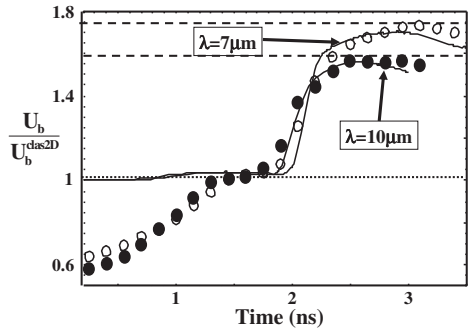

FIG. 5. Ratio of the bubble velocity to the classical value using the bubble velocity from the simulation for a perturbation with $\lambda = 10\ \mu$m (solid circles), $\lambda = 7\ \mu$m (open circles), and the analytic formula from Eq. (1) (solid line). The dashed lines are given by Eq. (4).

the ratio of the bubble penetration velocity U_b into the target to the classical value. The simulation results (circles) are compared to the analytic formula Eq. (1) (solid lines), using the vorticity as plotted in Fig. 4. At $t = 0$, the bubble penetration velocity is the sum of the ablation velocity and the initial velocity perturbation. Notice that the bubble velocity first reaches a plateau at the classical value of about 1.4 ns. Then, as the RTI vortex reaches the bubble tip, the bubble velocity rises well above the classical value. Using Eq. (1) and Fig. 4, the peak value of the bubble velocity in direct drive can be approximated with the following simple formula:

$$U_b^{\text{peak2D}} \approx \sqrt{\frac{g(1 - r_d)}{3k} + \frac{V_a^2}{r_d}}. \qquad (4)$$

During the nonlinear phase, the bubble density for $\lambda = 10$ and $7\ \mu$m is close to the linear theory prediction of $\rho_l = 0.6$ g/cm^3 ($r_d \approx 0.15$) and $\rho_l = 0.7$ g/cm^3 ($r_d \approx 0.17$), leading to a peak bubble velocity of $U_b^{\text{peak2D}} \approx 11.4$ and $10.2\ \mu$m/ns higher than the classical value of 7 and $5.8\ \mu$m, respectively, and in agreement with the simulations (dashed lines in Fig. 5). It is likely that the single-mode bubble acceleration discussed here will affect the predictions of the multimode bubble front penetration. This can be assessed by comparing multimode simulations of the same density profiles with and without ablation. This effect is weaker for CH ablators in direct-drive ICF due to their lower ablation velocity and higher r_d.

The authors thank Dr. I. Igumenshchev of LLE for confirming our numerical results with his hydro code. This work has been supported by the U.S. Department of Energy under Cooperative Agreements No. ER54789 and No. DE-FC03-92SF19460.

---

*Present address: E.T.S.I. Aeronauticos, Universidad Politecnica de Madrid, Spain.

[1] J. D. Lindl, *Inertial Confinement Fusion* (Springer, New York, 1998).

[2] Lord Rayleigh, *Scientific Papers II* (Cambridge University Press, Cambridge, England, 1900), p. 200.

[3] J. Sanz, Phys. Rev. Lett. **73**, 2700 (1994); R. Betti *et al.*, Phys. Plasmas **3**, 2122 (1996).

[4] H. Takabe *et al.*, Phys. Fluids **28**, 3676 (1985); R. Betti *et al.*, Phys. Plasmas **5**, 1446 (1998).

[5] J. Sanz *et al.*, Phys. Rev. Lett. **89**, 195002 (2002); T. Ikegawa and K. Nishihara, Phys. Rev. Lett. **89**, 115001 (2002); J. Garnier *et al.*, Phys. Rev. Lett. **90**, 185003 (2003).

[6] D. Layzer, Astrophys. J. **122**, 1 (1955); K. Mikaelian, Phys. Rev. Lett. **80**, 508 (1998); V. N. Goncharov, Phys. Rev. Lett. **88**, 134502 (2002).

[7] V. N. Goncharov, Phys. Rev. Lett. **82**, 2091 (1999); A. L. Velikovich and G. Dimonte, Phys. Rev. Lett. **76**, 3112 (1996).

[8] P. Clavin and L. Masse, Phys. Plasmas **11**, 690 (2004).

[9] P. W. McKenty *et al.*, Phys. Plasmas **8**, 2315 (2001).